Available online at www.sciencedirect.com
SCIENCE DIRECT®
Vision Research 46 (2006) 2691–2702
Vision Research
www.elsevier.com/locate/visres

Evidence for elongated receptive field structure for mechanisms subserving stereopsis

Chien-Chung Chen [a,b], Christopher W. Tyler [a,*]

[a] The Smith-Kettlewell Eye Research Institute, 2318 Fillmore Street, San Francisco, CA 94115, USA
[b] Department of Psychology, National Taiwan University, 1, Sec. 4, Roosevelt Rd. Taipei 106, Taiwan

Received 3 August 2005; received in revised form 24 January 2006

Abstract

To study the spatial extent and shape of the binocular disparity mechanisms subserving depth perception, we employ the spatial summation paradigm of contrast threshold for front/back depth discrimination at a fixed binocular disparity. The stimuli were Gabor patches with disparity set at either 4 or 8 arcmin and spatial frequency set at an optimal value of 4 cy/deg. Contrast threshold was measured as a function of length and width of the Gabor patches to determine the aspect ratio of greatest efficiency. The space constant of the Gaussian envelope varied between 0.0375° and 0.9° in either vertical or horizontal directions, or both simultaneously. For vertical elongation of the Gabor patches, discrimination sensitivity improved by 4–6 dB for a doubling of the length of the Gabor patches, then reduced more slowly as the length further increased. However, extending the Gabor patches horizontally across cycles produced little or no sensitivity improvement. Instead, discrimination performance collapsed in a fashion that is incompatible with many models of disparity processing. The results imply that the main mechanisms subserving stereoscopic depth discrimination are vertically elongated for vertical-bar Gabors and encounter special difficulties integrating horizontal disparity information. Disparity discrimination sensitivity for very small targets was also much greater than predicted by the single-mechanism fit, implying the presence of a second, independent mechanism with a very small summation field, which may underlie the fine stereoscopic processing system.

Keywords: Depth discrimination; Linear filter; Disparity; Luminance contrast; Detection

1. Introduction

It is a common view that disparity processing in the visual system is a multistage process (Fleet, Wagner, & Heeger, 1996; Julesz, 1971; Mayhew & Frisby, 1978; Ohzawa, 1998; Tyler, 1990; Qian & Andersen, 1997). The first stage contains spatial-frequency-selective linear filters modeled after the receptive fields of the simple cells. The function of this stage is to analyze the luminance contrast in the image in each eye. The outputs of the corresponding linear filters from both eyes are then integrated together for a disparity computation.

The receptive field structure of the luminance filters plays a major role in disparity computation. The sensitivity profile of the luminance specific RFs is known to be well fit by a Gabor function, which is the product of a Gaussian envelope and a sinusoid (Marcelja, 1980; Daugman, 1985; DeAngelis, Ohzawa, & Freeman, 1991; Jones & Palmer, 1987). The luminance filters feeding particular disparity mechanisms may have different receptive field (RF) structure for the left and right eyes, encoding the disparity in the image. Horizontal disparity may be signaled either by a phase difference (DeAngelis et al., 1991; Ohzawa, DeAngelis, & Freeman, 1996) or a position difference (Anzai, Ohzawa, & Freeman, 1999; Prince, Cumming, & Parker, 2002) between these pairs of RFs.

To complement the issue of disparity coding in the RF, there has been much study of the spatial frequency, phase and position tuning of the luminance filters. However,

* Corresponding author. Fax: +1 415 3458455.
E-mail address: cwt@ski.org (C.W. Tyler).

0042-6989/$ - see front matter © 2006 Published by Elsevier Ltd.
doi:10.1016/j.visres.2006.02.009

there is little empirical data on the shape and the spatial extent of the RFs for disparity processing in human observers. This information is essential for an understanding of how stereoscopic system sums information across space in individual retinal images and the accuracy of the disparity computation (Marr, 1982; Mayhew & Frisby, 1978; Tyler, 1975). There is psychophysical evidence that the global properties of the RF, such as size (Hess, Kingdom, & Ziegler, 1999; Prince & Eagle, 1999, 2000; Wilcox, Elder, & Hess, 2000), play a role in disparity computation. Indeed, Nienborg, Bridge, Parker, and Cumming (2004) suggest that the acuity limit for cyclopean depth modulation can be explained by the response properties of V1 neurons when stimulated by cyclopean disparity targets. This analysis is consistent with the fact that the sensitivity for cyclopean depth modulation peaks at about 0.4 cy/deg, regardless of the size of the summation field for disparity modulation (Tyler & Kontsevich, 2001), although deviations from this generality have been reported for extreme values of the carrier spatial frequency (Hess et al., 1999).

In this study, we measured the summation field for disparity processing for both horizontal and vertical directions in terms of the luminance contrast threshold for depth discrimination. The summation fields may be interpreted in terms of the structure of the underlying filters involved in disparity processing. The extent of the RF of a filter is often characterized by the critical size of a relevant stimulus beyond which performance improvement levels out (Kelly, 1975; Polat & Tyler, 1999; Sekiguchi, Williams, & Brainard, 1993). Hence, in our experiment, the luminance contrast threshold should decrease with the increase of the stimulus size until a critical point, then level out at the point where the summation of disparity information reaches the limit for the RFs mediating discrimination performance.

One extra benefit of this paradigm is that it allows direct comparison of the summation fields for disparity discrimination with those for luminance detection. If the disparity computation directly takes input from the linear filters, we would expect that they should share the same spatial properties. However, the best luminance contrast filters may not necessarily be the ones that feed the stereoscopic mechanisms. Hence, in addition to the spatial summation along the modulation direction, we also measured the summation along the along the collinear direction of the stereoscopic Gabor patches, and in both directions simultaneously, in order to characterize the two-dimensional properties of the mechanisms underlying disparity discrimination.

Prince and Eagle (2000) showed that depth discrimination performance for Gabor stimuli decreased as the envelope size of luminance Gabor stimuli increased. The critical envelope size, where the observer performance fell to chance level, was between 2 and 4 cycles of the carrier wave in horizontal extent. This experiment seems to imply that an increment in stimulus size increases the likelihood for false matching in the disparity computation. Hence, in addition to the extent of the RF, the false matching in the horizontal direction could provide a further constraint on the summation of disparity information across space. In order to test for this possibility, we included a condition in which the Gabors were replaced by simple Gaussian blobs (corresponding to the Gabor envelope with a zero spatial frequency carrier). The simple Gaussian is not subject to the false matching problem because it has only one peak in each eye; any effects that are similar to those for the Gabors cannot be subject to the false matching problem, and must be attributable to some other aspect of the stereoscopic processing (cf. Kontsevich & Tyler, 1994).

2. Methods

2.1. Stimulus

Fig. 1 shows a diagram of the stimulus display. Two Gabor patches were presented to each eye, one in the upper left and the other in the lower right quadrant of the display. A circular fixation point of 3′ radius in the center of the display defined the origin $(0,0,0)$ of the image/disparity coordinates. The luminance at a point (x,y,d) on the display is defined by

$$\mathrm{ML}(x,y) = L_{\mathrm{bg}} * (1 + C * \cos(2\pi f(x \pm h_x)) * \exp((x \pm h_x)^2/\sigma_x^2) * \exp((y \pm h_y)^2/\sigma_y^2))$$

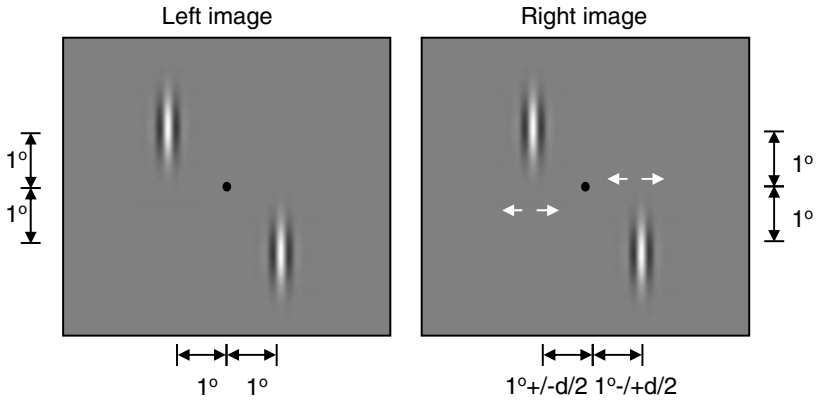

Fig. 1. A diagram of the spatial configuration of the experimental display. Arrows represent the disparity shift.

for the left eye image and

$$\mathrm{MR}(x,y) = L_{\mathrm{bg}} * (1 + C * \cos(2\pi f(x \pm h_x \pm d/2)) * \exp((x \pm h_x \pm d/2)^2/\sigma_x^2) * \exp((y \pm h_y)^2/\sigma_y^2))$$

for the right eye image. The parameter L_{bg} is the mean luminance of the display, 35 cd/m^2; C is the contrast of the Gabor patch and f is the spatial frequency, 4 cy/deg. The displacements h_x and h_y denote the distance from the fixation to the center of the Gabor patch at zero disparity. The values of h_x and h_y were 1° except for the two large-area conditions, in which they were 2°. The disparity d was either 4′ or 8′, which are approximately 90° and 180° phase disparity, respectively, for the 4 cy/deg pattern. The upper left and the lower right Gabor patches shifted by $d/2$ in opposite directions to produce a percept that one patch was closer to the observer than the other without any net lateral or disparity shift. In terms of a contrast-energy model of depth processing (DeAngelis et al., 1991; Fleet et al., 1996; Ohzawa et al., 1996), the 90° condition should provide the optimal depth discrimination (cf. Simmons & Kingdom, 1994).

In the depth discrimination task, the parameters σ_x and σ_y controlled the size of the Gabor patches in the horizontal (modulation) and in the vertical (collinear) direction. There were three conditions of size variation. In the height condition, the value of σ_x was held constant at 0.15°, while σ_y was varied from 0.0375° to 0.9°. In the width condition, the value of σ_y was 0.15° while σ_x was varied from 0.0375° to 0.9°. In the area condition, $\sigma_x = \sigma_y$ and both parameters changed in tandem from 0.15° to 0.9°.

It may seem that the 8′ disparity condition (which produced a phase-shift of ~180°) should provide no depth discrimination because each monocular bar has matching bars equidistant on either side in the other eye to provide local disparities that are equally near and far (except for those at the two edges of the patch). Hence the stimulus is ambiguous with respect to near and far disparities. We therefore analyzed the local stereo processing of extended Gabor patches with a position disparity between the two eyes (schematized for an uncrossed disparity in an orthogonal Keplerian diagram in Fig. 2A). The schematic assumes that disparity is processed when the contrast of any bar exceeds a particular threshold. The left eye (L) and right eye (R) Gabors appear in Fig. 2A as checked strips depicted above and below the frontoparallel line (diagonal), respectively. The map of disparity activations is depicted in the Keplerian array diagram of Fig. 2B. The horizontal and vertical lines represent the lines of sight to each Gabor element, passing through their locations on the frontoparallel lines. The projected sensitivity zones of disparity-selective units are represented as circles.

There has to be some process to remove the ambiguous disparities from consideration, since we only see one depth along any given line of sight (the uniqueness constraint of Marr, 1982). A straightforward version of this constraint is to assume cancellation between disparity activations symmetric around the horopter (left diagonal in Fig. 2A) regardless of their luminance polarity (see Tyler, 1975, 1990). Implementing this constraint (gray disks) leaves the map of unique disparity activations in Fig. 2C (black disks). It is clear that these activations are all on the uncrossed (far) side of the horopter. This kind of model illustrates how disparity information is available from disparate Gabor patches, even when the luminance carrier is at a 180° phase shift.

2.2. Apparatus

The stimuli were presented on two Mitsubishi Diamond Scan 15″ monitors, one for each eye, each driven by an IXMicro ProRez graphic board. A Macintosh computer controlled the graphic boards and response processing. The viewing field was 10.7° (H) by 8° (V). The resolution of the monitors was 640 horizontal by 480 vertical pixels, giving 60 pixel per degree at the viewing distance used (128 cm). The refresh rate of the monitor was 66 Hz. We used the LightMouse photometer (Tyler, 1997) to measure every level of the input/output intensity function of the monitor. This information allowed us to compute linear lookup table settings to linearize the output within 0.2%.

2.3. Procedures

We used a spatial two-alternative forced-choice (2AFC) paradigm to measure the luminance contrast threshold for disparity discrimination. In each trial, one Gabor patch in the right eye image shifted in disparity by $d/2$ while the other shifted by $-d/2$. A random number generator determined which patch was given the positive disparity. The task of the observer was to decide which of the two patches looked closer. We used the Ψ minimum entropy threshold-seeking algorithm (Kontsevich & Tyler, 1999) to measure the luminance contrast threshold, defined as the luminance contrast that produced 75% correct depth discrimination. There were 40 trials for each threshold measurement. Each reported datum point was an average of 4–8 repeated measures.

Three observers participated in this study. CC is an author of this paper and TS and AK were paid observers naïve to the purpose of the study. All three observers had corrected to normal (20/20) visual acuity and normal stereoacuity.

3. Results

3.1. Summation for Gabor at 4′ disparity

Fig. 3 shows the luminance contrast thresholds for depth discrimination at 4′, or approximately 90° phase,

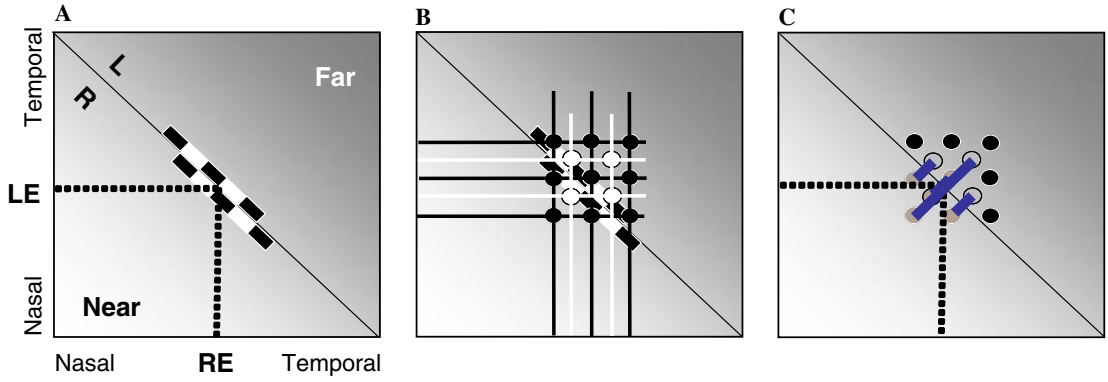

Fig. 2. Diagram to explain how the observer can perform depth discrimination with 180° phase disparity. (A) The 180° stimulus in the orthogonalized binocular projection, shown for the case of far disparity. The black and white rectangles represent the sign of the luminance modulation in a three-cycle Gabor in the left (L) and right (R) stimuli. The diagonal line denotes the frontoparallel plane at zero disparity. (B) The bars project to the two retinas along sets of projection lines that generate a grid of spurious correspondences (circles), each of which would activate a disparity-selective neuron with a stereoscopic receptive field tuned to the spatial location of the circle. (C) Line-of-sight inhibition symmetrical about the horopter would suppress the effect of the symmetric pairs of spurious correspondences, leaving a V-shaped set of locations that would be exclusively biased in the far direction (black circles).

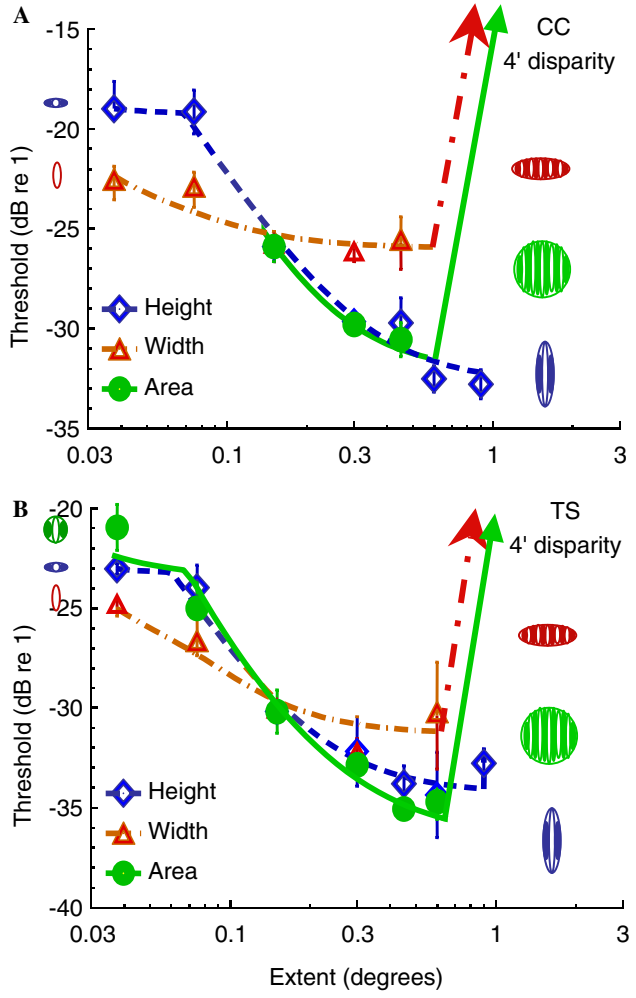

Fig. 3. Luminance contrast threshold for disparity discrimination with Gabor patches at 4′ disparity (~90° phase disparity). Blue diamonds and dashed curve denote thresholds for the vertical length condition, red triangles and dashed-dot curve denote the horizontal width condition and green circles and solid curve denote the area condition. The smooth curves in the figure are fits of the two-mechanism model discussed in the text. (A) Observer CC; (B) observer TS. Error bars are 1 SEM.

disparity. The smooth curves in the figure are fits of the model discussed below. The blue diamonds and dashed curve denote threshold for the vertical length condition and the red triangles and dashed dot curve denote the horizontal width condition. The two functions are anchored at the same value for the one-cycle Gabor patch with $\sigma_x = \sigma_y = 0.15°$, where the half-height full width (HHFW) is one wavelength of the carrier wave. For both observers, the contrast threshold decreased as the height of the Gabor patch increased. From the one-cycle anchor point, there was a 6–8 dB decrease in threshold, corresponding to a 2- to 2.5-fold increase in sensitivity, as the height increased 4-fold.

On the other hand, increase in width from the anchor point did not have much effect on contrast threshold. For increasing width, the greatest threshold reduction was 0.39 dB for CC and 2.1 dB for TS, not significant for CC ($t(6) = 0.46$, $p = 0.33 > 0.01$) or for TS ($t(6) = 2.42$, $p = 0.026 > 0.01$). Beyond the point of maximum reduction, however, threshold increased rapidly (arrows in Fig. 3) and the observers could not discern a disparity difference for σ_x greater than 0.6°, or a HHFW larger than three wavelengths of the carrier wave. For greater widths, the observers failed to achieve the criterion level of depth discrimination at even the highest contrast level that our apparatus could produce. This failure of depth discrimination with the wide stimuli is consistent with the stereoacuity results of Hess and Wilcox (1994) and Prince and Eagle (2000), but the difficulties of its interpretation will be considered in Section 5.

The above result suggests that the RFs for disparity discrimination have a vertically elongated shape. Hence, the observer can utilize extra information provided by increases in height but not by increases in width. If this were the case, one would expect that increasing both the height and the width of the Gabor patch would have the same effect on threshold as an increase in height alone. The area condition data, shown as the green circles and solid curve in Fig. 3, demonstrate this behavior. The threshold increases for the area condition, where the height and the width covaried, were about the same as for the height condition, where the width was constant. When the height and width increased beyond four cycles, however, the observers were again unable to perform depth discrimination with the large width patches. Evidently the increase in height for these isotropic patches was not able to overcome the defect introduced by the width increase, which therefore represents a hard limit for disparity processing regardless of stimulus size.

One issue that has never been addressed in spatial summation studies is the effect of the converse manipulation of decreasing the height and the width of the Gabor patches from the isotropic anchor point to Gabors of *less* than one cycle. Fig. 3 shows that the result of this manipulation was an increase in the contrast thresholds for depth discrimination (by a total of 7 dB for CC and 8 dB for TS). A reduction in height produced a greater increase in contrast threshold than the corresponding width reduction. Hence, the stereoscopic system is more efficient in using height than width information within the one-cycle range. It is curious, however, that there was almost no threshold change for reduction of σ_y below 0.075°, implying a plateau at the low end of the height condition curve (although equipment limitations precluded measurement of sizes below 0.04°). This deviation from a linear threshold increase for small sizes is seen in every subject and in every height condition tested. It may not always be a plateau relative to the next size tested, but it is always an improved performance relative to the proportional increase predicted from the single mechanism model. Thus, the plateau cannot be modeled by a single mechanism summation function and its significance in terms of the underlying neural processing will be discussed later in the paper.

3.2. Summation for Gabors at 8′ disparity

Fig. 4 shows the luminance contrast threshold for depth discrimination at a larger disparity of 8′, or approximately 180° phase, disparity. Again, the smooth curves in the figure are fits of the model discussed below. The blue diamonds and dashed curve denote threshold for the length condition, the red triangles and dashed dot curve denote the width condition, and the green circles and solid curve denote the area condition. Depth discrimination for 8′ disparity was almost identical to that for 4′ disparity. Increasing height from the one-cycle anchor stimulus showed about a 6 dB improvement in threshold, or a twofold increase in sensitivity, while increasing width produced little, if any, change. As in Fig. 3, a summation effect similar to the height effect was observed by increasing the height and the width together. At the lower sizes, we again observed the 'plateau' in both observers when the height was small, implying that performance was not degraded by a factor of two reduction in the size of the stimulus. Conversely, when the width of the Gabor patches was increased beyond 0.5° the observers completely failed to discriminate depth at 8′, about the same limit as for the 4′ disparity condition. Thus, the measured characteristics of the summation behavior were essentially unaffected by a doubling of the disparity.

3.3. Summation for Gaussian blobs

To test whether the bars within the Gabors were indeed contributing to depth discrimination, one can remove the bars to leave a simple Gaussian luminance blob as the test stimulus. Fig. 5 shows the depth discrimination with Gaussian blobs at 8′ disparity (Fig. 5A) and 4′ disparity (Fig. 5B), with the same coding conventions as for Figs. 3 and 4. Notice that the anchor stimulus has $\sigma_x = \sigma_y = 0.035°$ rather than 0.15°, matching the envelope of the smallest Gabor stimulus used in the above experiments. As mentioned above, the 0.15° anchor point for the Gabor stimuli was designed such that the half-height width of the envelope was 1 period of the carrier wave. For the Gaussian stimuli, we did not have this constraint. Hence, we used the smallest stimulus as the anchor point to maximize the threshold reduction from the level of the anchor point.

Qualitatively, the results for the Gaussian blobs were strikingly similar to those for the Gabor patches.

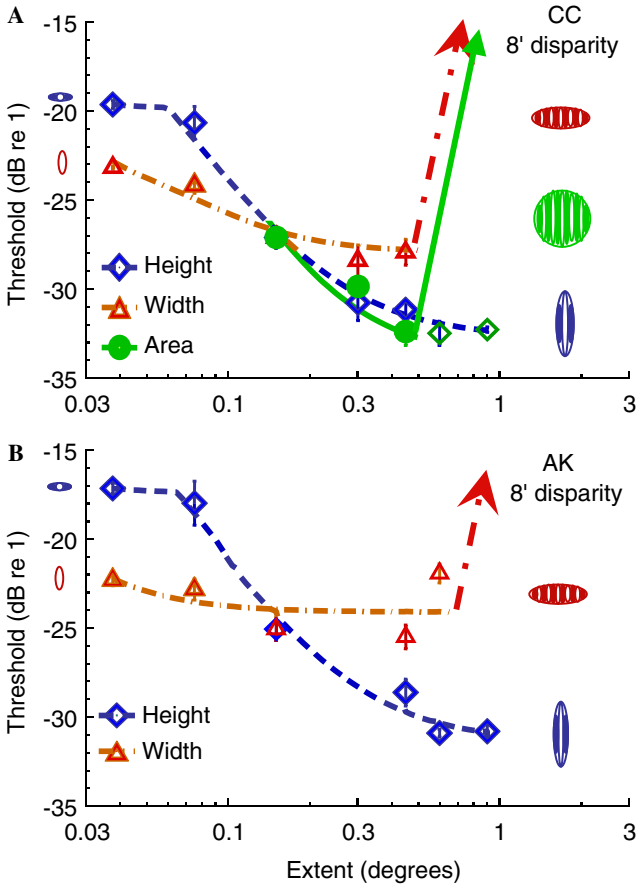

Fig. 4. Luminance contrast threshold for disparity discrimination with Gabor patches at 8′ disparity (~180° phase disparity). Coding conventions as in Fig. 3. (A) Observer CC; (B) observer AK.

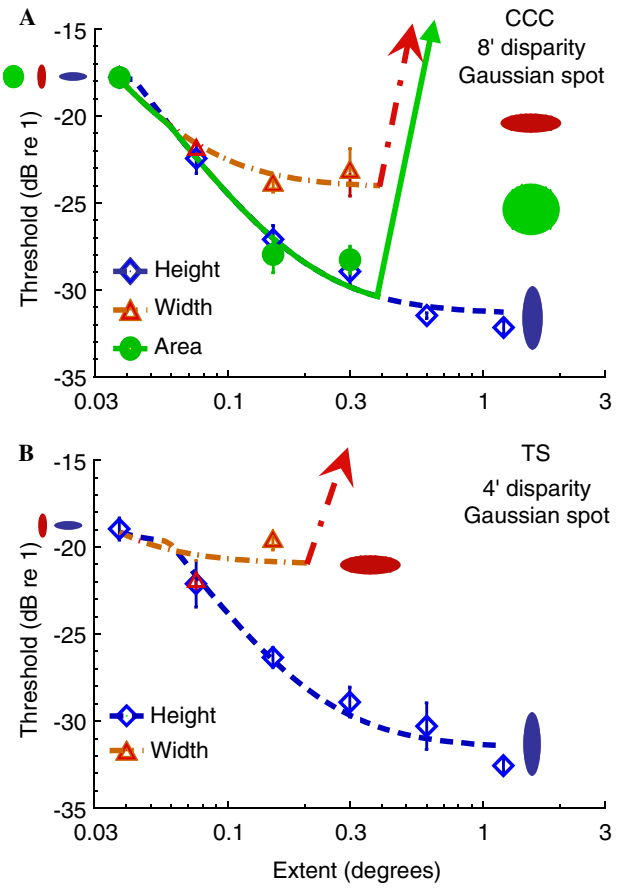

Fig. 5. Luminance contrast threshold for disparity discrimination with Gaussian blobs at 8′ disparity (A) and at 4′ disparity (B). Coding conventions as in Fig. 3. (A) Observer CC; (B) observer TS.

Increasing the height of the stimulus reduced the threshold by 12 dB for TC and 14 dB for CC dB (blue curves in Fig. 5). These values correspond to a 4–5 times increment in sensitivity, which is about the same as the overall threshold reduction from the shortest to the longest Gabor. An increment in width had much less effect: the greatest width effect was 3 dB for TS and 5.5 dB for CC (red curves in Fig. 5). In addition, most of the threshold reduction for width occurred between the first two points. Checking the area condition for observer CC (green curve in Fig. 5) again showed that it had a similar effect to the height condition, suggesting that the receptive field of the filter that was responsible for the depth discrimination with Gaussian blobs was again quite elongated vertically.

Beyond the asymptote for improvement with width, depth discrimination failed entirely when the Gaussian width was between 0.3° and 0.6°, similar to but slightly lower than the result with Gabor patches. This similarity in threshold behavior when the luminance bar structure was removed from within the stimulus envelope implies that the increase in threshold has no relation to the false matching problem, because there are no false matches in the case of simple Gaussian profiles. However, the Gaussian introduces a different problem that the spatial frequency content is shifted to lower frequencies in proportion to its width, which may account for the small discrepancy between the location of the collapse in the Gabor and Gaussian conditions. There seems to be no stimulus that would probe the summation width at a fixed vertical spatial frequency without introducing some other artifact.

The other issue to consider in interpreting the Gaussian disparity thresholds is the luminance gradient reduction as the size increases. However, this property of the Gaussian stimuli should be considered in the context that such a gradient decrease is characteristic of all plausible receptive-field models, which typically use Gaussian or sinusoidal elements whose slopes get shallower in proportion to their scale. There is no reason to suppose that disparity-selective RFs deviate from this property. Indeed the Gabor formalism is the preferred descriptor of their sensitivity profiles (Cumming & Parker, 1999, 2000; Cumming & DeAngelis, 2001; DeValois, Albrecht, & Thorell, 1982; Ohzawa, 1998; Ohzawa & Freeman, 1986a, 1986b; Prince et al., 2002). In this formalism, the optimal Gaussian stimulus is one that fits the center lobe of the Gabor weighting function. Importantly, the best fitting Gaussian scales proportionately with the scale of the Gabor, producing proportionately scaled activation. Thus, the larger Gaussians will generate a proportionately larger response in neurons with proportionately scaled RFs. Any loss due to increasing the width of the Gaussians must therefore reflect a lack of proportionately larger RFs available for disparity processing.

4. Analysis

4.1. Summation model and data analysis

We used a two-dimensional linear filtering model to estimate the size of the RF of the disparity-selective neuron most sensitive to each left/right stimulus pair (with the neuron conceptualized as residing in cortical area V1). For simplicity of computation, we assume that attention was focused on the RF mechanism most relevant to the discrimination, i.e., that the linear filters have the spatial frequency, orientation and phase selectivity matching the spatial properties of the stimulus. The RFs are presumed to be binocular and to have a range of possible disparities around the stimulus disparity. The only free parameters to be estimated are those of the shape and size of the most sensitive RF envelope (i.e., its horizontal and vertical extent). In this model, the ith RF is described by the Gabor function

$$\Theta_i(x,y,d\prime) = \cos(2\pi f(x \pm d\prime/2)) * \exp((x \pm d\prime/2)^2/s_{x,i}^2) * \exp(y^2/s_{y,i}^2),$$

where d' is the disparity between the RFs in the two eyes, f is the spatial frequency, i is the sample from the set of possible RF shapes and sizes, and $s_{x,i}$ and $s_{y,i}$ are the scale parameters to be estimated for the Gaussian envelope of the ith mechanism. The scale parameters $s_{x,i}$ and $s_{y,i}$ for the filters should not be confused with σ_x and σ_y which denote the scale parameters of the Gaussian envelope of the stimuli.

The mechanisms are binocular, with one RF for the left eye and one for the right. For simplicity of computation, we assume that the spatial profile of the left and the right eye RFs are the same except for a horizontal displacement d'. The greatest response of this mechanism occurs when the left eye image has the same spatial configuration as the left RF and the right eye image, whose retinal position deviates from the left eye image by disparity d, matches the right RF. The RF for each eye acts like a linear filter. For the left eye image, the response of the ith RF, $\Theta_{I,L}(x,y)$, assumed to have the same spatial configuration as the stimulus, is given by the two-dimensional integral of the product of the stimulus and the ith RF. For the case of Gabor function stimuli and RFs, this integral permits an analytic solution, as exemplified by that for the left eye stimulus:

$$\begin{aligned} E_{i,\mathrm{L}} &= \int\int \Theta_{i,\mathrm{L}}(x,y)L(x,y)\mathrm{d}x\,\mathrm{d}y. \\ &= w_{i,\mathrm{L}} * C * [s_y^2\sigma_y^2/(s_y^2+\sigma_y^2)]^{1/2*}[s_x^2\sigma_x^2/(s_x^2+\sigma_x^2)]^{1/2} \\ &\quad * (1+\exp((2f\pi)^{2*}(s_x^2+\sigma_x^2)/s_x^2\sigma_x^2)) \\ &= w_{i,\mathrm{L}} * C * f_i(s_x,s_y), \end{aligned}$$

where $w_{i,\mathrm{L}}$ is a weight coefficient, C is the contrast of the Gabor patch and $f_i()$ is the filter characteristic determined by the size of the stimulus. Here, and in the subsequent text where the reference to an RF is clear, we omit the subscript

i for s_x and s_y only for ease of reading. We are not implying s_x and s_y to be the same for all RFs.

The corresponding derivation applies for $E_{i,\mathrm{R}}$ for the right eye. Changing the spatial phase or spatial frequency of the stimulus will have an influence on the weight w_i but not the filter characteristic $f_{\mathrm{i}}(s_x, s_y)$. The weight w_i would also decrease with the spatial offset between the RF and the stimulus. A detailed derivation of this result is discussed elsewhere (Chen & Tyler, 1999). The disparity computation mechanism is assumed to sum the linear filter responses from the two eyes and square the sum to produce disparity energy E_i. That is

$$E_i = (E_{i,\mathrm{L}} + E_{i,\mathrm{R}})^2 = g_d * C^2 * f_i(s_x, s_y)^2,$$

where the sensitivity $g_d = (w_{i,\mathrm{L}} + \mathrm{w}_{i,\mathrm{R}})^2$ and the subscripts L and R denote the left and right eye inputs.

Notice that g_d is a nonlinear combination of the w_i's. Hence, like the w_i's, its value depends on the position difference between the stimulus and the RF and, in turn, depends on the disparity of the left and the right images. Different disparity conditions, such as the 4′ and 8′ settings, should yield different values of g_d while stimuli with different sizes but the same disparity should have the same value for g_d. The model assumes that the threshold is determined by the most relevant disparity computation mechanism at each image location. In our spatial 2AFC experiment, depth discrimination can be achieved when the response of any mechanism for each of the two intervals reaches a critical level (Tyler & Chen, 2000). That is, threshold is reached when

$$R = \max(E_i(-d/2), E_i(d/2)), \quad i = 1, 2, \ldots, n$$

reaches a critical value.

Because a single-mechanism version gave a poor fit, the fit of the model with $n = 2$ spatial filter mechanisms is the form used for Figs. 2–4. The functions were fit with different initial values for space parameters of the two mechanisms (the points where the threshold curves leveled out for the first mechanism and the points where the threshold curves showed the initial plateau for the second mechanism). It should be emphasized that the response from all filters must be identical for the width and height functions for the isotropic stimulus, since it is common to both functions. This is an inherent constraint in the 2D model that may not be obvious from inspection of the fitted functions, which are 1D cuts through the full 2D fit.

This two-mechanism model explains as much as 94–97% of threshold variation in the data. The parameters of the fits are provided in Table 1, scaled in arcmin. The parameters $s_{x,i}$ and $s_{y,i}$ are the scale parameters of the fitted filter Gaussian envelopes. The residual root mean square error (RMSE) was only 0.65 dB for CCC, 0.92 dB for TS, and 0.81 dB for AK. These RMSE values are less than or close to the standard errors of measurement of 0.68 dB for CCC, 1.06 dB for TS, and 0.57 dB for AK. It is obvious from the data that the larger mechanism is elongated vertically. The height-to-width ratio ranged from 1.98 to 7.27 across observers and Gabor stimulus conditions, averaging 3.59 for the Gabor conditions and 8.29 for the Gaussian conditions.

Table 1
Estimated receptive field size

Observer	Stimulus	Receptive field 1		Receptive field 2	
		$s_{x,1}$	$s_{y,1}$	$s_{x,2}$	$s_{y,2}$
Gabor					
CC	4′ Gabor	4.36′	19.15′	0.36′	0.49′
	8′ Gabor	5.42′	15.38′	0.48′	0.59′
TS	4′ Gabor	6.27′	12.43′	0.12′	0.55′
AK	8′ Gabor	2.61′	18.98′	0.48′	0.29′
Average		4.66′	16.74′	0.36′	0.48′
SD		±1.58′	±3.50′	±0.17′	±0.13′
Gaussian					
CC	8′ Gaussian	0.47′	11.82′	4.03′	1.94′
TS	4′ Gaussian	2.57′	13.37′	1.64′	1.07′
Average		1.52′	12.60′	2.83′	1.51′
SD		±1.48′	±1.10′	±1.69′	±0.62′

One noteworthy feature of the fit is that data for all but the lowest envelope widths (a FWHH of 0.0375°) are well fit by the larger of the two mechanisms in the model. This single-mechanism fit applies to the whole range in which the spatial frequency is defined. Below about half a cycle in extent, the envelope is so narrow that the carrier frequency ceases to be a meaningful parameter—the Gabor effectively becomes a Gaussian blob. The implication of the single-mechanism fit over this range is thus that, rather than a range of filter sizes and shapes for processing binocular disparity at the spatial frequency tested, there is only one operative filter for all stimulus extents (in the range where the spatial frequency is defined). We may therefore infer that, for the defined spatial frequency, neurons of only one RF size and shape are involved in disparity processing.

4.2. Two mechanisms?

The main motivation underlying the two-mechanism model plotted in the figures derived from the fact that all our observers showed evidence of a plateau in the threshold functions when the height factor (σ_y) of the Gabor patch was smaller than 1.5° regardless of the disparity tested, implying lower thresholds for the narrow stimuli than would be predicted from a single-mechanism model. As shown in Fig. 6A, a single mechanism model cannot account for this plateau, but continues to show a threshold increase in proportion to the reduction in height or width. The plateau is best explained by the combination of a larger mechanism that determines the threshold for stimuli with a height factor greater than 1.5° and a smaller mechanism for stimuli with a height factor below this level (Fig. 6B). The smaller stimuli can only occupy a minor proportion of a large RF. Hence, the large mechanism cannot respond to a small stimulus effectively, implying the existence of a smaller RF that can respond efficiently to the

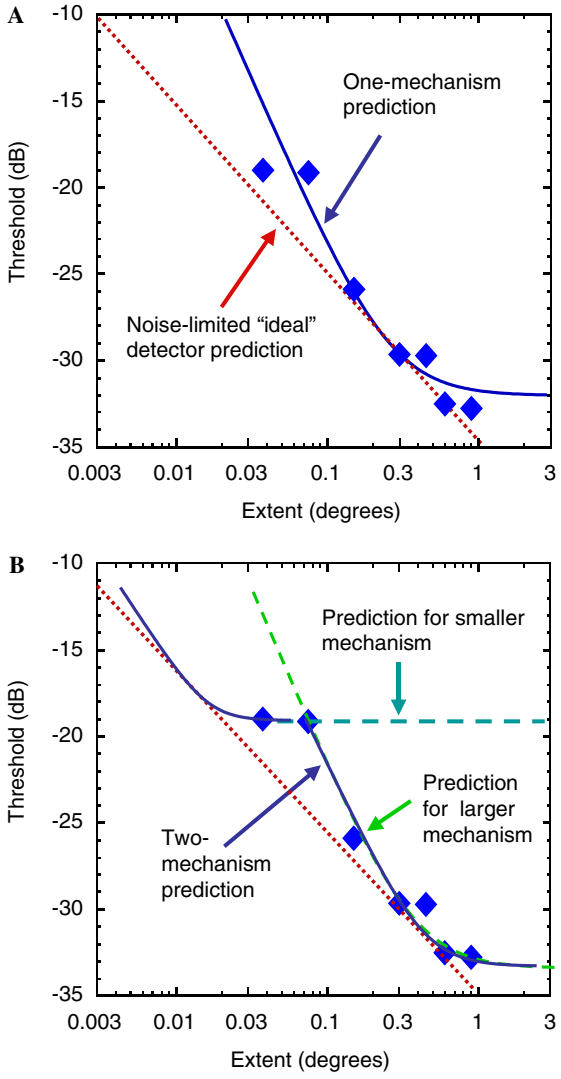

Fig. 6. (A) Fit (blue curve) of the one-mechanism model, which completely misses the thresholds for the smallest stimuli. The red dotted lines (A and B) with a slope −0.5 on this log–log plot denote the ideal observer prediction, which is the envelope of an infinite number of mechanisms, limited by the same local input noise as is assumed for each mechanism of the two-mechanism model. (B) Fit (blue curve) of the two mechanism model that captures the characteristics of the data. The dashed green curves denote the functions for the two underlying mechanisms that give this two-mechanism fit. The datum points were taken from Fig. 3A.

small stimuli. Moreover, the smaller stimuli used in this experiment are evidently large enough to extend beyond the range of a small RF to generate the observed plateau at the tail-end of their response.

The two-mechanism model fits significantly better than the one mechanism model. The RMSE dropped 38–55% with the addition of the second mechanism to the model. Even with the extra three parameters (s_x, s_y, and g_d) considered, the improvement of the fit is statistically significant for CC ($F(3,30) = 4.49$, $p = 0.0002$, <0.01) and TS ($F(3,15) = 6.62$, $p = 0.0046 < 0.01$). Similarly, the two-mechanism model may be compared with the Ideal Observer model, which would imply improvement with the square root of stimulus area (as found for dynamic random-dot stimuli by Tyler & Julesz (1980)). The Ideal Observer model implies the existence of disparity processing mechanisms matching every stimulus extent (Tyler & Chen, 2000), which is a much less parsimonious system than one with only two mechanisms, which would severely degrade the model fit relative to the two-mechanism model that we assess here. For good measure, we also compare the two-mechanism model with a model of arbitrary uniform slope as a free parameter for each condition for each observer (in addition to the sensitivity parameter that is a variable for all mechanisms). Though conceptually simple, this form of fit does not correspond to a straightforward RF model of the underlying processing mechanisms.

Taken across all conditions, the RMSE of the two-mechanism model is 0.74 dB. For the arbitrary slope model, the RMSE is much higher at 1.24 dB. Strictly speaking, these models cannot be compared because they do not have nested parameters, but if they were nested the uniform slope model would provide a significantly worse fit at $p < 0.001$ ($f(18,51) = 5.12$), even taking the extra three parameters (s_x, s_y, and g_d) of the two-mechanism model into consideration. Accordingly, the Ideal Observer model, with a fixed slope that derives from a coherent analytic framework, provides a significantly worse fit again, with an RMSE of 2.31 dB ($f(12,51) = 10.51$, $p < 0.001$). (The Ideal Observer model is a nested version of the two-component model, since it is derived as having a mechanism matching every stimulus configuration, amounting to a seven-mechanism model for most of the present data sets.)

Thus, the two-mechanism model provides a fit that is significantly better than the one-mechanism model, than the Ideal Observer slope of −1/2, or even than a fit with an arbitrary slope for each data set. Although the last model is not a nested version of the two-mechanism model, it is a classic default fit that needs to be excluded before a multi-component model is considered. The fit of the two-mechanism model is comparable with the standard error of the data measurement, and the fact that it accounts for such a high proportion of the variance (94–97%) implies that it provides a good description of the mechanisms underlying the detection performance.

5. Discussion

5.1. Receptive field size

In the literature on two-dimensional spatial vision, the RFs were estimated to have elongation ratios of 1.2–1.6 in some contrast detection (Watson, Barlow, & Robson, 1983; Daugman, 1985) or hyperacuity (Wilson, 1986) experiments. Recently, a study by an international consortium (Carney et al., 2000) with data in 16 observers from 10 laboratories showed that the length of the estimated RF is not statistically significantly different from its width, i.e., an elongation ratio of 1.0. This study is particular relevant to the current one, for the stimuli used in both studies were

very similar (4 cy/deg Gabor) and there was an overlap of observers.

The vertical elongation ratio of the primary estimated RF for disparity discrimination ranged from about 2–7 across observers and Gabor stimulus conditions, with a mean of about 4. This is much greater elongation than the ratio estimated in the two-dimensional spatial vision literature. The clear implication of this result is that the RFs underlying human disparity processing are more elongated than those for spatial luminance processing (which presumably includes the subset of binocular cells with no disparity preference and perhaps those with a preference for zero disparity as well). Thus, disparity processing activates a different neural substrate, and is not just a comparison between monocular examples of the spatial processing filters (cf. Read & Cumming, 2003). Such differences presumably reflect the different demand characteristics for determining the depth distances of different parts of the visual field, as opposed to their luminance structure.

While the height estimates for the vertically elongated RF for the Gaussian spot and Gabor patches are similar, the estimated width for the Gaussian fit is substantially smaller than that for the Gabor. There are two possible explanations. First, the spatial frequency content of the Gaussian spots and the Gabor patches are quite different. It is likely that the Gaussian spot probes the excitatory region of the RF. In this regard, the strongest activation of a Gabor RF by a Gaussian stimulus can be shown to occur when the σ_x is about 0.18 of the carrier wavelength, corresponding to 2.76 arcmin at 4 cy/deg for the estimated Gabor filter size. This prediction is not significantly different from the measured values, given the error of the fits. The other possibility is that the Gaussian stimuli are processed by different spatial frequency channels which in turn possess different sizes, but this hypothesis is not needed given the fit to the single-mechanism prediction.

5.2. The two-mechanism analysis

We may conclude from the values in Table 1 that the horizontal and vertical size parameters for the smaller mechanism are both very small, as is also seen from the plotted functions in Fig. 5B. The implication of these data is that the smaller mechanism, at 2–3′ FWHH is essentially limited by the extent of optical blur on the retina. This small disparity-selective RF would be well-suited for disambiguating depth structure in complex stimuli like random-dot stereograms. The two-mechanism interpretation is thus consistent with the original conception of Julesz (1971), that there is a fine disparity mechanism for complex, detailed disparity images and a coarse disparity mechanism for simple processing of larger disparities. Our data provide no evidence about the complexity or relative disparity selectivity of these two mechanisms, but they strongly support the idea of two (widely separated) size ranges and provide further characterization of their two-dimensional structure.

5.3. Alternative explanations

In our model, the elongation property is implemented as an attribute of the first-order linear filter. This type of model is consistent with those proposed in many contrast detection studies (Daugman, 1985; Watson et al., 1983). However, there are other possibilities. For instance, changing the length of a Gabor patch changes the contrast energy more than changing the width. This is qualitatively consistent with our result that increasing the length of the Gabor stimulus decreases threshold faster than increasing the width while decreasing the length of the Gabor stimulus increases threshold faster than decreasing the width. However, qualitative similarity does not imply quantitative equivalence. Our isotropic Gabor stimulus was well-balanced between the positive and the negative regions. The contrast energy for the Gabor with length doubled was only 2% more than the Gabor with width doubled while the threshold difference was easily 3–4 dB or 40–60% difference. Moreover, the contrast energy difference cannot explain the results with Gaussian spots. After all, the Gaussian spot has no carrier wave; increasing the width or the length of the Gaussian spot will produce the same increment in contrast energy. Yet, we observed a clear threshold advantage for increasing the length vs. the width.

Similarly, there are models proposing that the first stage of visual image processing has isotropic linear filters operating on every location of the input image. That is, mathematically, the output of the first stage is the convolution between the filters and the input image (e.g., Adelson, Simoncelli, & Freeman, 1991; Watt, 1988). In this type of model, the threshold is determined by a linear (e.g., Watt, 1988) or nonlinear (e.g., a contrast energy model) summation of the convolutions. These types of models, while able to show a difference for Gabors with different elongation, have no inherent property to implement the elongation of summation for a Gaussian spot in the vertical (or in the horizontal) direction.

To make this type of model express the elongation property for Gaussian spots, one may assume that the summation mechanism that pools the outputs from linear filters sums more filter outputs in the vertical direction than in the horizontal. Such anisotropic summation is not implausible. Chen and Tyler (1999) measured the contrast detection threshold for a string of Gabor patches. The phase of each Gabor element was either the same as or opposite from that of its neighbors. The contrast detection thresholds for the alternate-phase string were equivalent to the thresholds for the same-phase string regardless the string length. This result suggests that, in addition to the mechanisms responding to the Gabor elements, there are summation mechanisms that sum local mechanism outputs after some nonlinear transform. The elongation of any such summation mechanism cannot be separated from the elongation of the linear filters in the present study. If the summation is linear, it is mathematically equivalent to having the threshold determined by an elongated linear filter. If

the summation is not linear, it will need a more complicated stimulus manipulation, such as that in Chen and Tyler (1999), than the current experiment to separate the linear filtering and the summation effect. This issue, however, is beyond the scope of the present paper.

5.4. Challenges to the disparity energy model

We find that the contrast threshold for disparity discrimination is limited by the Gaussian envelope size, whether or not it has luminance modulation within it. The results are similar for Gabor patches and Gaussian blobs that have no carrier wave, not only in the shapes of the summation functions, but in the fact that the depth discrimination completely failed when the width of the stimuli was greater than 0.45° to 0.6° (arrows in Figs. 3–5), which is a replication of the effect reported by Hess and Wilcox (1994) and Prince and Eagle (2000). Given our test conditions this means at least a 10- fold (AK) to 20- fold (CC) fold increase in threshold for at most a one-octave increase in spatial extent. This rise corresponds to collapse in discrimination performance with a slope of at least 5–10 on log–log coordinates, far beyond the slope of one for the width effect in stereoacuity reported by Schor, Wood, and Ogawa (1984). Hess and Wilcox (1994) showed that this collapse of performance was consistent with a limit based on envelope size rather than either carrier spatial frequency or number of cycles in the envelope, although the failure of discrimination to be supported by a (second-order) envelope-based mechanism for wider envelopes was not explained.

We note that this kind of collapse in performance may be unique to the stereoscopic system because all other position tasks (vernier, orientation, motion, etc.) have recourse to the neural resources of the entire brain to resolve the position change. These include second-order contrast mechanisms, third-order attention mechanisms, memory mechanisms, and so on. Empirical evidence reveals the absent of collapse in performance in contrast detection up to 64 cycles (Graham, Robson, & Nachmias, 1978), and in optical flow detection up to 70° (Burr, Morrone, & Vaina, 1998). Stereo position correspondence, on the other hand, has to be established *before* the site of binocular convergence, which is generally considered to be the input layer of the primary visual cortex. Beyond this point of convergence, disparity position differences between the inputs from the two eyes are lost, so there is no recourse to higher-order mechanisms for the disparity comparison.

The disparity processing models currently postulated in the literature (DeAngelis et al., 1991; Fleet et al., 1996; Ohzawa et al., 1996; Read & Cumming, 2003) cannot explain this paradoxical collapse in disparity discrimination. In such models, at least for 4′ disparity Gabor patches, larger stimuli have more luminance modulation and thus more information for a contrast energy computation. Hence, the depth discrimination should not fail for wide stimuli in the context of the disparity energy model (DeAngelis et al., 1991; Fleet et al., 1996; Ohzawa, 1998; Read & Cumming, 2003). To solve this problem, one could postulate an inhibitory lobe outside the normal disparity-energy computing region. However, the catastrophic failures that we measured imply that the inhibitory lobe would have to be very steep and narrow. The difference-of-Gaussian form that is commonly used for modeling inhibition lobes (Enroth-Cugell & Robson, 1966; Phillips & Wilson, 1984; Rodieck, 1965) cannot handle such a steep sensitivity loss.

The other possible explanation of this catastrophic failure in depth discrimination is an inability to make local comparisons in larger stimuli when the threshold is limited by a Gaussian envelope. For larger stimuli, the luminance gradient of the Gaussian envelope may be too shallow to give enough contrast between the two corresponding locations in each eye and thus fail to provide necessary disparity cues in small RFs. This hypothesis fits our result of the horizontal size limit and the inference of smaller disparity mechanisms. However, it postulates a highly localized RF that cannot detect luminance changes within a few minutes of arc but yet can extract the Gaussian envelope that is up to a several degrees wide in detection studies. Such a mechanism could account for the catastrophic collapse of discriminability at a limiting stimulus width only by assuming that the local contrast comparisons are themselves compared across the two sides of the Gaussian by a push–pull mechanism with a specific spatial extent. Widening the stimulus would not only make all the gradients shallower, it would move the optimal stimulus gradients beyond the spatial range of the comparison mechanism, magnifying the difficulty of comparing the gradients. Thus, a disparity comparator of defined spatial extent seems to be the only hypothetical mechanism compatible with the sudden collapse of depth discrimination capability for horizontal extension of the Gabor stimuli.

This analysis makes it clear that the catastrophic collapse of disparity discrimination provides stringent constraints on the type of mechanism underlying disparity processing. We show how it excludes several popular proposals and offer the plausible alternative of a defined spatial comparator mechanism, although novel paradigms will need to be developed to put this alternative to the test.

6. Summary

1. Contrast thresholds for depth discrimination of Gabor targets at one spatial frequency are well fit by a two-mechanism model with small isotropic and large anisotropic receptive field types.
2. The larger receptive field is vertically elongated by an average ratio of 4:1, more anisotropic than typical estimates of the receptive field structure underlying contrast detection.
3. The horizontal extent is restricted by a hard limit at about 30′ width, beyond which there is a catastrophic collapse of disparity discrimination that is incompatible with disparity energy models.

4. The large-field mechanism is insensitive to the presence of luminance modulation within the Gabor envelope, showing similar characteristics for Gaussian blob stimuli.
5. The small, isotropic summation field was on the scale of the optical blur of the retinal image, and may underlie the fine stereoscopic processing system.

Acknowledgment

This work was supported by NEI 7890 to C.W.T.

References

Adelson, E. H., Simoncelli, E. P., & Freeman, T. (1991). Pyramids and multiscale representations. In A. Gorea, Y. Fregnac, Z. Kapoula, & J. Findlay (Eds.), *Representations of Vision*. Cambridge: Cambridge University Press.

Anzai, A., Ohzawa, I., & Freeman, R. D. (1999). Neural mechanisms for encoding binocular disparity: Receptive field position versus phase. *Journal of Neurophysiology, 8*, 874–890.

Burr, D. C., Morrone, M. C., & Vaina, L. M. (1998). Large receptive fields for optic flow detection in humans. *Vision Research, 38*, 1731–1743.

Carney, T., Tyler, C. W., Watson, A. B., Makous, W., Beutter, B., Chen, C. C., et al. (2000). Modelfest: First year results and plans for year two. *SPIE Proc., 3959*, 140–151.

Chen, C. C., & Tyler, C. W. (1999). Spatial pattern summation is phase insensitive in the fovea but not in the periphery. *Spatial Vision, 12*, 267–285.

Cumming, B. G., & DeAngelis, G. C. (2001). The physiology of stereopsis. *Annual Review of Neuroscience, 24*, 203–238.

Cumming, B. G., & Parker, A. J. (1999). Binocular neurons in V1 of awake monkeys are selective for absolute, not relative, disparity. *Journal of Neuroscience, 19*, 5602–5618.

Cumming, B. G., & Parker, A. J. (2000). Local disparity not perceived depth is signaled by binocular neurons in cortical area V1 of the macaque. *Journal of Neuroscience, 20*, 4758–4767.

Daugman, J. G. (1985). Uncertainty relation for resolution in space, spatial frequency, and orientation optimized by two-dimensional visual cortical filters. *Journal Optical Society of America A, 2*, 1160–1169.

DeAngelis, G. C., Ohzawa, I., & Freeman, R. D. (1991). Depth is encoded in the visual cortex by a specialized receptive field structure. *Nature, 352*, 156–159.

DeValois, R. L., Albrecht, D. G., & Thorell, L. G. (1982). Spatial frequency selectivity of cells in macaque visual cortex. *Vision Research, 22*, 545–559.

Enroth-Cugell, C., & Robson, J. G. (1966). The contrast sensitivity of retinal ganglion cells of the cat. *Journal of Physiology, 187*, 517–552.

Fleet, D. J., Wagner, H., & Heeger, D. J. (1996). Neural encoding of binocular disparity: Energy models, position shifts and phase shifts. *Vision Research, 36*, 1839–1857.

Graham, N., Robson, J. G., & Nachmias, J. (1978). Grating summation in fovea and periphery. *Vision Research, 18*, 815–825.

Hess, R. F., Kingdom, F. A., & Ziegler, L. R. (1999). On the relationship between the spatial channels for luminance and disparity processing. *Vision Research, 39*, 559–568.

Hess, R. F., & Wilcox, L. M. (1994). Linear and nonlinear filtering in stereopsis. *Vision Research, 34*, 2431–2438.

Jones, J. P., & Palmer, L. A. (1987). An evaluation of the two-dimensional Gabor filter model of simple receptive fields in cat striate cortex. *Journal of Neurophysiology, 58*, 1233–1258.

Julesz, B. (1971). *Foundations of Cyclopean Perception*. Chicago: University of Chicago Press.

Kelly, D. H. (1975). Letter: How many bars make a grating? *Vision Research, 15*, 625–628.

Kontsevich, L. L., & Tyler, C. W. (1994). Analysis of stereothresholds for stimuli below 2.5 c/deg. *Vision Research, 34*, 2317–2329.

Kontsevich, L. L., & Tyler, C. W. (1999). Bayesian adaptive estimation of psychometric slope and threshold. *Vision Research, 39*, 2729–2737.

Marcelja, S. (1980). Mathematical description of the responses of simple cortical cells. *Journal Optical Society America, 70*, 1297–1300.

Marr, D. (1982). *Vision*. San Francisco: Freeman.

Mayhew, J. E., & Frisby, J. P. (1978). Stereopsis masking in humans is not orientationally tuned. *Perception, 7*, 431–436.

Nienborg, H., Bridge, H., Parker, A. J., & Cumming, B. G. (2004). Receptive field size in V1 neurons limits acuity for perceiving disparity modulation. *Journal of Neuroscience, 24*, 2065–2076.

Ohzawa, I. (1998). Mechanisms of stereoscopic vision: the disparity energy model. *Current Opinion in Neurobiology, 8*, 509–515.

Ohzawa, I., DeAngelis, G. C., & Freeman, R. D. (1996). Encoding of binocular disparity by simple cells in the cat's visual cortex. *Journal of Neurophysiology, 75*, 1779–1805.

Ohzawa, I., & Freeman, R. D. (1986a). The binocular organization of simple cells in the cat's visual cortex. *Journal of Neurophysiology, 56*, 221–242.

Ohzawa, I., & Freeman, R. D. (1986b). The binocular organization of complex cells in the cat's visual cortex. *Journal of Neurophysiology, 56*, 243–259.

Phillips, G. C., & Wilson, H. R. (1984). Orientation bandwidths of spatial mechanisms measured by masking. *Journal Optical Society of America A, 1*, 226–232.

Polat, U. ., & Tyler, C. W. (1999). What pattern the eye sees best. *Vision Research, 39*, 887–895.

Prince, S. J., Cumming, B. G., & Parker, A. J. (2002). Range and mechanism of encoding of horizontal disparity in macaque V1. *Journal of Neurophysiology, 87*, 209–221.

Prince, S. J. D., & Eagle, R. A. (1999). Size-disparity correlation in human binocular depth perception. *Proceedings of the Royal Society of London B, 266*, 1361–1365.

Prince, S. J., & Eagle, R. A. (2000). Stereo correspondence in one-dimensional Gabor stimuli. *Vision Research, 40*, 913–924.

Qian, N., & Andersen, R. A. (1997). A physiological model for motion-stereo integration and a unified explanation of Pulfrichlike phenomena. *Vision Research, 37*, 1683–1698.

Read, J. C., & Cumming, B. G. (2003). Testing quantitative models of binocular disparity selectivity in primary visual cortex. *Journal of Neurophysiology, 90*, 2795–2817.

Rodieck, R. W. (1965). Quantitative analysis of cat retinal ganglion cell response to visual stimuli. *Vision Research, 5*, 583–601.

Schor, C. M., Wood, I. C., & Ogawa, J. (1984). Spatial tuning of static and dynamic local stereopsis. *Vision Research, 24*, 573–578.

Sekiguchi, N., Williams, D. R., & Brainard, D. H. (1993). Efficiency in detection of isoluminant and isochromatic interference fringes. *Journal Optical Society of America A, 10*, 2118–2133.

Simmons, D. R, & Kingdom, F. A. (1994). Contrast thresholds for stereoscopic depth identification with isoluminant and isochromatic stimuli. *Vision Research, 34*, 2971–2982.

Tyler, C. W. (1975). Spatial organization of binocular disparity sensitivity. *Vision Research, 15*, 583–590.

Tyler, C. W. (1990). A stereoscopic view of visual processing streams. *Vision Research, 30*, 1877–1895.

Tyler, C. W. (1997). The Morphonome image psychophysics software and a calibrator for Macintosh systems. *Spatial Vision, 10*, 479–484.

Tyler, C. W., & Chen, C. C. (2000). Signal detection theory in the 2AFC paradigm: Attention, channel uncertainty and probability summation. *Vision Research, 40*, 3121–3144.

Tyler, C. W., & Julesz, B. (1980). On the depth of the cyclopean retina. *Experimental Brain Research, 40*, 196–202.

Tyler, C. W., & Kontsevich, L. L. (2001). Stereo-processing of cyclopean depth images: Horizontally elongated summation fields. *Vision Research, 41*, 2235–2243.

Watson, A. B., Barlow, H. B., & Robson, J. G. (1983). What does the eye see best? *Nature, 302*, 419–422.

Watt, R. J. (1988). *Visual processing: Computational, psychophysical, and cognitive research*. Hillsdale: Erlbaum.

Wilcox, L. M., Elder, J. H., & Hess, R. F. (2000). The effects of blur and size on monocular and stereoscopic localization. *Vision Research, 40*, 3575–3584.

Wilson, H. R. (1986). Responses of spatial mechanisms can explain hyperacuity. *Vision Research, 26*, 453–469.